Experiments on the MHD Effect on the Drainage of a LiPb Channel and Supporting Numerical Computations with the Level Set Method

Radiological source terms estimation for the Divertor Tokamak Test (DTT) facility

Samuele Meschini[a], Raffaella Testoni[a]*, Giorgio Maddaluno[b]

[a]*Dipartimento Energia "Galileo Ferraris", Politecnico di Torino, Corso Duca degli Abruzzi, 24 – Torino, Italy*

[b] *ENEA, Italian National Agency for New Technologies, Via Enrico Fermi, 45 - Frascati, 00040, Italy*

Abstract

The Divertor Tokamak Test (DTT) facility will start its operations in 2026. DTT will operate with D-D fuel only, for an expected operational period of 25 years. Nevertheless, tritium will be produced by the D(d,p)T reaction. A mandatory step in the safety assessment of the machine is the estimation of the different source terms. Major contributions to the source terms are due to tritium and to activated dust. The amount of tritium in the vacuum chamber, in co-deposited tungsten layers and implanted in the bulk of the first wall is computed in this work. Also, a preliminary estimation of dust production due to inter and intra ELMs sputtering is carried out. Results report small amount of source terms related to tritium, below 1 mg after one year of full power operations, and less than 300 g of activated dust at the end of life.

Keywords: DTT, source terms, tritium, activated dust, safety

*Corresponding author: raffaella.testoni@polito.it

1. Introduction

The DTT (Divertor Tokamak Test) facility is an infrastructure included in the European roadmap for fusion that will contribute to the demonstration of fusion energy feasibility. DTT integrates research into physics and technology to support ITER (International Thermonuclear Experimental Reactor) during the operational phase and DEMO (Demonstration Fusion Power Plant) during the design phase. The main goals of DTT are the investigation of possible solutions for the disposal of thermal loads on plasma facing components and test of advanced materials. The project was proposed in 2015, and DTT is expected to start operations in 2026 at the ENEA (Italian National Agency for New Technologies) Frascati Research Centre. The current design of DTT foresees a First Wall (FW) and a divertor made of tungsten. Different divertor configurations might be tested during the experimental campaigns (e.g., liquid metal divertors). The present works considers tungsten plasma facing materials with a single null configuration.

DTT will operate with D-D (Deuterium-Deuterium) fuel mixtures only, with an average plasma density $n_e = n_D = 1.8 \cdot 10^{20} m^{-3}$. A small amount of tritium is expected to be produced in the machine due to the D(d,p)T reaction. Additionally, activated dust will be produced during DTT operations. In the framework of DTT safety analysis a source term quantification is carried out in this work. This kind of analysis is mandatory for licensing the machine, and all the possible radiological source terms must be taken into account. The assessment considers tritium in gaseous form in the vacuum chamber during the shots, tritium in re-deposited tungsten layers, tritium implanted in the bulk material of FW and divertor and activated dust.

In this paper the typical operative annual scenario is assumed to be characterized by 6 months of experimental activities and 6 months of stop for maintenance and modification. In these 6 months, the operational agenda foresees 4 days/week of operations, with 6 shots/day. The duration of each shot is 100 s, while the maximum performances are achieved for 50 s per shot [1].

The analysis is part of a two-steps approach for the estimation of DTT source terms. A preliminary quantification is carried out based on the available data on DTT design and operations, by taking advantage also of the results from experimental campaigns in other relevant machines. The main goal is to provide conservative, reasonable values of the main source terms for DTT. A detailed analysis will follow as the design and the operating conditions of DTT proceed, exploiting state-of-the-art plasma-surface interaction codes (e.g., ERO [2], WallDYN [3]) that can leverage a higher level of detail of the machine parameters.

The paper is structured as follows: Section 2 introduces the main design parameters for DTT, Section 3 describes the methodology and the assumptions, Section 4 presents the results, Section 5 discusses the results with respect to DTT safety goals and Section 6 draws the conclusions.

2. Description of the DTT facility

DTT facility is designed to explore different divertors and plasma configurations relevant for ITER and DEMO, in order to mitigate the risk associated to thermal loads in DEMO. Specifically, DTT will investigate a) divertor geometries and magnetic flux maps able to reduce the normal heat flux on the target, b) removal of plasma energy before it reaches the target by means of impurity radiation and c) recycling of particles released by the wall and increase of the density close to divertor plates to achieve a detached condition [1]. The experimental campaign is expected to start in 2026 for at least 25 years of operations. Figure 1 shows the timeline for DTT operations. *Phase 0* is devoted to the installation of the machine components. *Phase 1* foresees plasma operations with 3 MW of ICRH (Ion Cyclotron Resonance Heating), 14.5 MW of ECRH (Electron Cyclotron Resonance Heating) and 10 MW of NBI (Nuclear Beam Injection) available. In *Phase 2* additional power will be installed based on the results from the previous phase. *Phase 3* will test different

magnetic configurations and divertor concepts. The main design parameters of the machine for the single null configuration (the baseline configuration for DTT) are reported in Table 1.

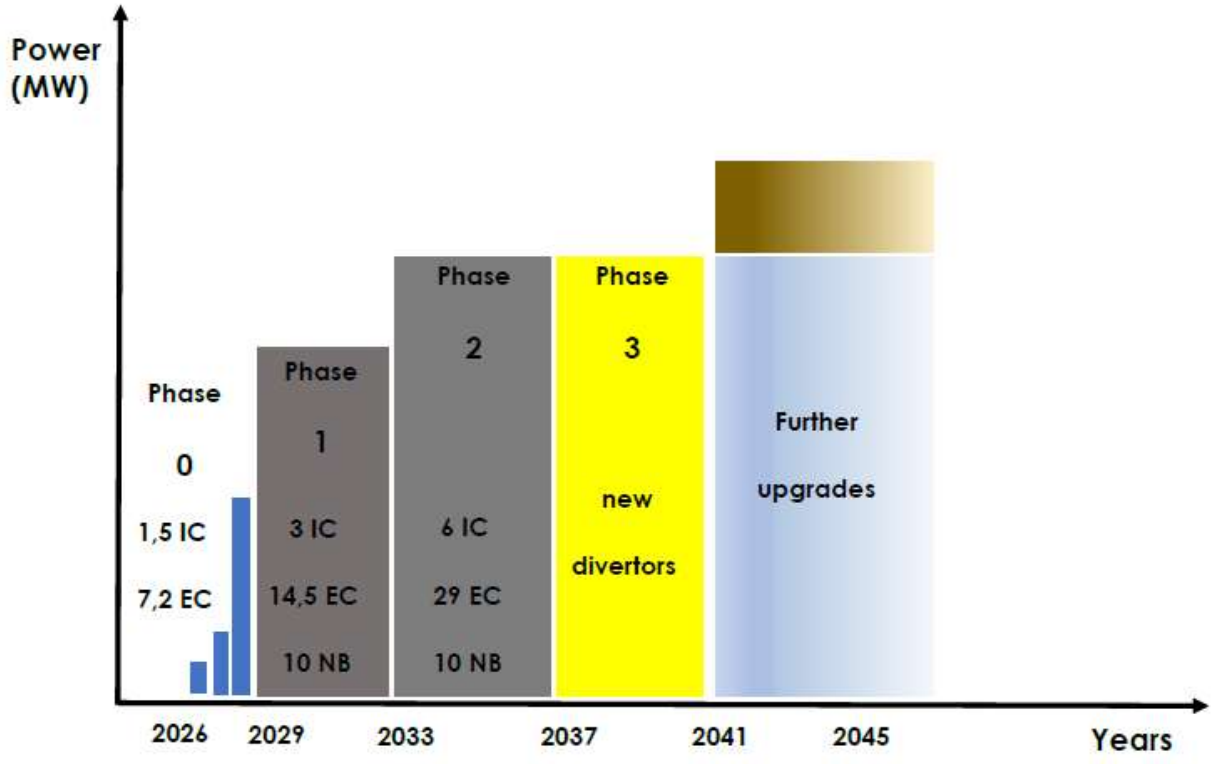

Figure 1 – DTT operational phases. At least 25 years of experimental campaigns are expected. The available heating power from different heating systems for each phase can be depicted (adapted from [1]**).**

Table 1 - Main DTT parameters for the single null configuration [1]**.**

Parameter	Value
R [m]	2.11
a [m]	0.64
R/a	3.3
V [m^3]	29
q_{95} [-]	3
I_p [MA]	5.5
B_T [T]	6.0
H_{98} [-]	1.0

S_{FW} [m^2]	66.8
S_{div} [m^2]	20
P_{div}[MW/m^2]	~10
dpa at EOL [-]	$2 \cdot 10^{-4}$
n_e [$10^{20} m^{-3}$]	1.8
T_e [keV]	6.1
$T_{e,div}$ [eV]	$5 \div 6$

R: major radius, a: minor radius, V: plasma volume, q_{95}: safety factor at 95% of minor radius, I_p: plasma current, B_T: toroidal magnetic field, H_{98}: confinement factor, S_{FW}: First Wall surface, S_{div}: divertor surface, P_{div}: divertor heat load, EOL: end of life, T_e: electron plasma temperature, n_e: electron plasma density.

3. Methodology

The methodology and the main assumptions made to carry out the source terms assessment are described in the present section. Tritium co-deposition and implantation, as well as dust production, belong to the much wider category of surface phenomena that take place in a fusion reactor. A detailed analysis of plasma-material interactions is beyond the scope of this work. Nevertheless, understanding the relevant phenomena is mandatory to justify the assumptions made for the calculations. High energy ions produce sputtered surface material atoms that may enter the plasma or re-deposit on the surface, generating re-deposited layers. Fuel can easily co-deposit in those layers up to saturation. The high energy ions impacting the surface may be reflected or may penetrate the surface material. Implanted ions migrate due to diffusion and permeation processes up to $\sim 100\ \mu m$ [4]. As for co-deposited fuel ions, saturation may occur on the first surface layers due to ions implantation. The surface material gets damage by ion and neutron bombardment, leading to defects formation. Hence, ions may also get trapped at defects. Furthermore, the gas present in the material merge in nucleation centres, producing bubbles. The interaction of all those phenomena makes the analysis extremely complex. Simplifying assumption are therefore needed before proceeding to a quantification of source terms.

A quite comprehensive overview of hydrogen retention in ITER plasma-facing materials can be found in [5], where the results from the coordinated research project dealing with hydrogenic retention in Be, C and W are described in detail. Depth profiles of D in W irradiated with 200-eV D^+ or exposed to 200-eV D^+ plasma allowed to identify three main zones of interest: the near-surface layer ($0.2 \div 0.5\ \mu m$ depending on ion energy), the subsurface layer ($0.5 \div 4\ \mu m$) and the bulk ($> 6\ \mu m$). D retention in W shows a strong dependence on temperature, varying by more than an order of magnitude in the temperature range of 300-800 K. W temperature also affects D saturation: at 300 K, D concentration reaches saturation for D^+ fluence above a threshold ($10^{23}\ D^+/m^2$ in the experiments reported in [5]), whereas no evident saturation is reached for a tungsten temperature of 500K. Finally, D retention in W is found to depend also on D^+ flux.
Below a flux threshold ($10^{18}\ D^+/(m^2 s)$ in the experiments reported in [5]) D diffusion outside the implantation zone balances the implanted ions, reaching a steady-state condition. For larger fluxes, the local concentration of deuterium may cause lattice distortion, leading to hydrogen trapping. Additional available data in literature comes from experimental machines, such as JET (Joint European Torus) [6][7], TFTR (Tokamak Fusion Test Reactor) [8][9], KSTAR (Korea Superconducting Tokamak Advanced Research) [10], JT-60U (Japan Torus-60 Upgrade) [8][11], Alcator C-Mod [9][12], Tore Supra [13], EAST (Experimental Advanced Superconducting Tokamak) [14] and ASDEX Upgrade (Axially Symmetric Divertor Experiment) [13][15][16][17]. It is recalled that tritium presence in DTT is due to the D-D reactions only. No D-T (Deuterium-Tritium) operations are planned. The triton energy resulting from D-D reaction is quite large, approximately 1 MeV. Most of these tritium ions are not slowed down and can penetrate deeply in the divertor [8][18]. Conversely, the small fraction of thermalized tritium ions is more likely to co-deposit within eroded materials.

In DTT, most of the expected erosion is localized on the divertor. In fact, the energy of ions impacting the FW is so low that no significant erosion is expected – at least in nominal operations. Similarly, the heat loads on the FW do not lead to significant W evaporation during nominal operations. A specific treatment is needed for transients such as ELMs (Edge Localized Modes) or disruptions, which may lead to tungsten ablation and additional dust production.

Focusing on the divertor, the erosion is mainly driven by impurity ions (Ne) and D ions impacting on its surface. The energy of incoming D ions is quite low, due to the low SOL (Scrape-Off Layer) temperature (20-30 eV). Furthermore, impurity ions mass is much larger than D mass, leading to higher sputtering yields during nominal operations. Nevertheless, the D ions energy impacting the divertor may rise as high as 1 keV during ELMs, overcoming the contribution from impurity ions flux [19]. No data is available on W ions produced by walls sputtering in DTT. Therefore, the self-sputtering contribution cannot be computed directly. A

preliminary estimate can be done by taking advantage of the results reported for JET-ILW (ITER-like wall) [20], where the operating conditions were similar to those expected in DTT. Approximately 20% of W gross erosion is due to self-sputtering. Thus, such as contribution is added to the calculation of W gross erosion.

As for the eroded W, the prompt redeposition probability is quite large. That is, because of the large Larmor radius of W ions, most of them hit the divertor surface before closing the first orbit. Still, there are further competing processes that complicate the behaviour of W ions [21]. Multiple ionizations reduce the W Larmor radius, whereas the Debye sheath accelerates the ion towards the surface. Therefore, the eroded material is deposited close to the erosion site, and simultaneous erosion and redeposition processes may occur, making the situation even more complex. For high-Z ions, such as tungsten, the prompt redeposition probability is quite large [22], at least for magnetic field lower than 10 T [21]. A prompt redeposition probability of 0.9 is assumed as reference value in this work. Tungsten ions that do not undergo to prompt redeposition are assumed to generate mobilizable dust.

A single divertor is considered in this analysis. This is consistent with the activation analysis from Villari et al. [23], which considered 28 years of irradiation for the FW and the divertor, and whose results are used to compute the radioactive source term associated to tungsten dust.

3.1 Tritium in the vacuum chamber

The amount of tritium [m^{-3}] present in the vacuum chamber in gaseous form (i.e., in the plasma) can be estimated by solving the equation:

$$\frac{dn_T}{dt} = \frac{1}{4} < \sigma v >_{DD} n_D^2 - < \sigma v >_{DT} n_D n_T - P \qquad (1)$$

where n_T and n_D are the tritium and deuterium concentration, $< \sigma v >_{DD}$ and $< \sigma v >_{DT}$ are the reaction rate for D-D and D-T reactions at 6.1 keV [1]. P is the amount of tritium removed from the pumping system. As a conservative assumption, P can be neglected. The equation is solved for $n(t)$, with $0 < t < 100\ s$ (i.e., for a pulse length). At the plasma operating conditions expected for DTT, $< \sigma v >_{DD} = 2.41 \cdot 10^{-25}\ m^3/s$, $< \sigma v >_{DT} = 2.01 \cdot 10^{-23}\ m^3/s$ [24] and $n_D = 1.8 \cdot 10^{20}\ m^{-3}$. It should be noted that the D-T reaction would probably not occur at 6.1 keV (i.e., tritons are not thermalized). As a matter of fact, $< \sigma v >_{DT} (T)$ varies by two orders of magnitude at most in the range 1 keV ÷ 1 MeV. Nevertheless, the contribution from the $< \sigma v >_{DT} n_D n_T$ term in Eq. (1) is much lower than the leading term, hence the resulting $n_T(t)$ is lowly affected by uncertainty on $< \sigma v >_{DT} (T)$. The reader should be aware that another possible contribution to T production in the vacuum chamber may come from beam-plasma interactions [25]. However, the quantification of T production from 400 keV D beams (as foreseen by the NBI system in DTT) is beyond the scope of this work.

3.2 Tritium in co-deposited tungsten layers

The co-deposition of tritium, with material eroded from the plasma-facing components in deposition-dominated areas is expected to be one of the main sources of tritium accumulation. Studies of tritiated co-deposited layers in TFTR [26] and JET [6] show that tritium is significantly retained inside the vacuum vessel due to the co-deposition of carbon eroded from plasma facing components. The surface analysis of JET ITER-like wall divertor described in [7] reports that the dominant region for fuel retention is the upper inner divertor, where co-deposits up to 40 μm were found after two experimental campaigns. This deposit was found to strongly adhere to the divertor tiles, limiting dust production from deposit disintegration. It is

important to note that this region was not affected by strong plasma interactions, with a surface temperature that usually did not exceed 300 °C. In [27], a systematic study of the influence of the deposition conditions (substrate temperature, deposition rate, energy of the incident particles) on the deuterium retention in co-deposited beryllium layers was carried out in PISCES-B (Plasma Interaction with Surface and Components Experimental Simulator). In particular, the combination of co-deposition and implantation seems the mechanism governing the deuterium co-deposition with beryllium. In addition, an equation to predict the Be co-deposits was derived and by means of this equation previously published data on retention in Be co-deposits are re-examined and relatively good agreement was found. As far as tritium co-deposition in tungsten is concerned, few studies are available in literature. It is expected that the tritium co-deposition with tungsten would be lower than carbon due to the lower sputtering yield. A reference study for deuterium co-deposited in tungsten is [28], where the influence of the deposition conditions on the deuterium retention in co-deposited tungsten layers formed both by magnetron sputtering and in the PISCES-B linear device was presented. In that study, the experimental parameters (e.g., tungsten deposition rate, the incident particle energy, the substrate temperature) were taken into account to explore the effect of deuterium retention in co-deposited tungsten layers. Starting from experimental data, an empirical relation was derived. Since the deposition conditions (temperature and deposition rates) appear to influence the deuterium retention in tungsten layers in the same way as for beryllium co-deposits [27], a similar empirical scaling is proposed to describe the D/W ratio with the deposition conditions [28]:

$$\frac{D}{W} = C \cdot r_d^{\alpha} \cdot E_n^{\beta} \cdot exp\left(\frac{\gamma}{T}\right) \tag{2}$$

where: C is a constant, r_d is the tungsten deposition rate, T is the substrate temperature during deposition, E_n is the average energy of the incoming particles on the surface. The different coefficients of Eq. (2) were determined by means of a regression analysis performed on all available data. In addition, in order to extend the validity of the correlation to future devices like ITER, the ratio between the flux of deuterium to tungsten atoms arriving at the substrate was introduced (Γ_D/Γ_W). The flux of deuterium atoms impinging on the substrate was estimated by using the measured current on the target and the reflection coefficient of deuterium ions on tungsten. The deposition rate varies with the relative arrival rate of deuterium and tungsten atoms: the higher Γ_D/Γ_W, the lower the deposition rate. Starting from these considerations, the derived equation is [28]:

$$\frac{D}{W} = 5.13 \cdot 10^{-8} \cdot \left(\frac{\Gamma_D}{\Gamma_W}\right)^{0.4\pm0.1} \cdot E_n^{1.85\pm0.4} \cdot exp\left(\frac{736 \pm 228}{T}\right) \tag{3}$$

where: $2 < \frac{\Gamma_D}{\Gamma_W} < 500$; $60\ eV < E_n < 280\ eV$; T is in K. it should be noted that in DTT $\frac{\Gamma_D}{\Gamma_W} \sim 0.03$ if Γ_W is considered to be produced by D and Ne sputtering. The amount of tritium (in co-deposited tungsten layers) that could be mobilized in case of accident can be assessed by following the recommendation from Holdren et al. [29], which set tungsten in the mobility category IV, that is, somewhat volatile under conditions that may be encountered in severe accidents. The maximum plausible release fraction ranges from $5 \cdot 10^{-4}$ to 0.1. Hence, as a conservative assumption, 10% of the tritium in co-deposited layer may be mobilized together with tungsten in case of severe accident.

3.3 Tritium implanted

Implanted tritium would penetrate the surface of the plasma facing components and migrate in the materials due to its high mobility [30]. Therefore, accurate assessment of tritium inventory in the first wall and divertor

caused by implantation is a crucial source term for licensing and safety purposes. A detailed model to assess the tritium depth profiles in plasma facing components have been developed by Sugiyama et al. [8]. Experimental validation demonstrated the validity of the model applied to Carbon components. Even if highly instructive, the model cannot be applied to tungsten-based components, such as those of DTT. Hence, a more general approach will be exploited for the estimation of tritium implanted in DTT plasma facing components. The amount of implanted fuel atoms can be roughly estimated with the following relation [22]:

$$M_T = m_T C_{TW} n_W S_W d_{imp} \tag{4}$$

where m_T is the tritium atomic mass, C_{TW} is the relative atomic tritium concentration in tungsten (T atoms/W atoms), n_W is the atomic density of tungsten, S_W is the wall surface, and d_{imp} is the average implantation depth. Note that C_{TW} is used alongside the text to indicate the relative atomic tritium concentration independently from the phenomenon under consideration (both co-deposition and implantation). Divertor conditions differ substantially from FW conditions. Hence, the source term related to tritium implanted is estimated separately for FW and divertor. The analytical estimation of C_{TW} is quite hard because of the many phenomena involved. Instead, many experiments dealing with hydrogen implantation are reported in literature. For this reason, the estimation for DTT is based on the experimental results reported in literature. Causey et al. [31] reported more than ten different implantation studies. In these studies, the concentration of deuterium ions in tungsten samples was assessed following deuterium bombardment at different fluences. Deuterium ions energy ranged between 100 eV and 30 keV, while tungsten sample temperature ranged between 350 K and 1000 K. Other relevant results are reported by Hatano et al. [4]. The energy range considered in these experiments is similar to the one reported by Causey et al. [31]. Conversely, the samples exploited in these studies were irradiated by a higher neutron fluence than the one expected in DTT. The concentration values reported in the different studies cover a wide range. Causey et al. [31] report values between $6 \cdot 10^{-5}$ and $1.5 \cdot 10^{-2}$, while Hatano et al. [4] report values between 10^{-2} for highly damaged samples and $3 \cdot 10^{-5}$ for lowly damaged samples. A plausible range of $C_{TW} = 10^{-2} \div 10^{-5}$ is considered in the following analyses.

3.4 Activated Dust

Large energy and particle fluxes are deposited onto wall elements in fusion experiments. Material is eroded mainly by physical sputtering in nominal conditions [22], but transient events such as ELMs and disruptions may lead to non-negligible tungsten ablation and consequent dust formation.

A quite comprehensive review of dust production in fusion devices can be found in [32]. Measurements from DIII-D [33], TFTR [9], Alcator C-Mod [9,12], JET [34], Tore Supra [35]–[37] and ASDEX-Upgrade [17] have been analysed, leading to the following conclusions. First, the average particle size is $2.8 \pm 2.4\ \mu m$. During severe accidents, these particles can be mobilized, and their dimensions make them easily transportable. Second, the similarity in dust size among different machines is a clear indication that dust production is ruled by similar processes, despite the different design and different operating parameters [32]. In the present work, material erosion due to physical sputtering and ELMs is considered for dust production. Material erosion due to disruptions is not considered.

Target atoms involved in the developing collision cascade may leave the surface if the received energy exceeds the surface binding energy E_s. Usually, the heat of sublimation as measured for real surfaces is used for the surface binding energy. Physical sputtering may be influenced by the target temperature due to a modification of the heat of sublimation. Specifically, the surface binding energy decreases with increasing target temperature. The sputtering yield due to the bombardment of ions onto the material surface depends

on the energy and angular distribution of the impinging particles, $Y_{ion \to W}(E, \theta)$. To take into account all the aforementioned processes, TRIM (Transport of Ions in Matter) code [38] has been exploited for the sputtering calculations. A conservative assumption can be made considering that all eroded material that does not undergo to prompt redeposition will become dust. Possible removal from pumping or cleaning processes is not considered.

A notable effort to model wall erosion in fusion reactors can be found in the work from Tokar [39]. The author developed a quasi-two-dimensional model to quantify DEMO first wall erosion taking into account physical sputtering from hot c-x neutrals (neutrals that participate to charge-exchange collisions), main and impurity ions. That model solves a transport problem for both neutral and charged plasma components in SOL, estimates the energy spectrum of the particles and quantifies wall erosion. In the present work, particle flux, mean energy and density have been taken from preliminary edge plasma simulations (performed with SOLPS-ITER) for the DTT reference configuration. Data is available only for the divertor targets. The divertor target has been discretized in 35 nodes on R-Z plane. As far as the FW is concerned, the sputtering yield and the ion flux has been extrapolated from the outer region of the divertor. Deuterium, tritium and neon ions bombardment were in the analysis. A Maxwellian distribution for the ion temperature was assumed. The highest mean energy of ions is found on the Low Field Side (LFS) divertor target, where $T_{mean} = 14.93\ eV$. The ionization states of Ne ions was accounted explicitly. The Debye sheath acceleration leads to an impact ion energy E_i computed according to $E_i = 3Zk_BT_e + 2k_BT_i$, for $T_e = T_i$, where T_e is the electron temperature, T_i is the ion temperature, Z is the electrical charge of the impinging ion and k_B is the Boltzmann constant. More than 300 TRIM simulations have been run by taking advantage of PySrim package [40]. Each run simulated 10^8 ions on a 10^4 Å thick tungsten surface. For each ion the energy was sampled from the corresponding Maxwellian distribution by means of the rejection method. A prompt redeposition probability $p = 0.9$ has been assumed. Hence, only 10% of the eroded particles contributes to dust production. The value $p = 0.9$ was chosen to provide a small conservative margin ($\sim 5\%$) with respect to experimental findings (e.g., post-mortem analysis in JET-ILW reported $p > 0.94$ [20]) in conditions similar to the ones expected in DTT. For full power years (i.e., from 9th to 28th year) the time considered for the dust production is $1.02 \cdot 10^4\ s$. That is, the average operations time has been computed from the equivalent time at full power operations ($2.49 \cdot 10^5\ s$ [1]) and scaled up or down according to the annual neutron yield [1]. This procedure makes the analysis consistent with the already developed neutronics analysis [23].

4. Results

4.1 Tritium in the vacuum chamber

The amount of tritium in the vacuum chamber during a shot has been computed according to Eq. (1). The calculations assume a deuterium density $n_D = 1.8 \cdot 10^{20}\ m^{-3}$ at $t = 0$. As a conservative assumption, the amount of tritium pumped out from the VV chamber has been neglected, as well as possible sink terms (e.g., tritium implanted). Hence, at the end of the shot, the concentration of tritium present in the vacuum chamber is $8.1 \cdot 10^{-7} g/m^3$. The mass of tritium is therefore $2.8 \cdot 10^{-5} g$ for a plasma volume of 34.502 m^3. It should be noted that this value of plasma volume is a conservative assumption. As a matter of fact, plasma volume changes during the shot. The value used for the calculations is the maximum volume during a shot in the single null scenario. Since this amount of tritium is in gaseous form, a mobilizable fraction of 100% should be considered in case of severe accident.

4.2 Tritium in co-deposited tungsten layers

Figure 2 shows the relative tritium concentration C_{TW} in co-deposited tungsten in the extrapolated range of the correlation (Eq. (3), $2 < \frac{\Gamma_D}{\Gamma_W} < 500;\ 60\ eV < E_n < 280\ eV$) [28]. Extrapolation is required because the ratio $\frac{\Gamma_T}{\Gamma_W}$ is much lower in DTT ($\frac{\Gamma_T}{\Gamma_W} \sim 0.03$). Similarly, for thermalized tritium ions ($T_{e,div} \sim 5 \div 6\ eV$) with impact energy $E_i \sim 30\ eV$, also E_i lays outside the range of the correlation. Hence, C_{TW} has been extrapolated down to reasonable values for DTT. The wall temperature T is set equal to 473 K for the first wall [1]. The divertor operating temperature has not been defined yet. However, thermal-hydraulics analyses suggest that the surface temperature will not exceed 1373 K. An operating window between 473 K and 1373 K is analysed for the divertor.

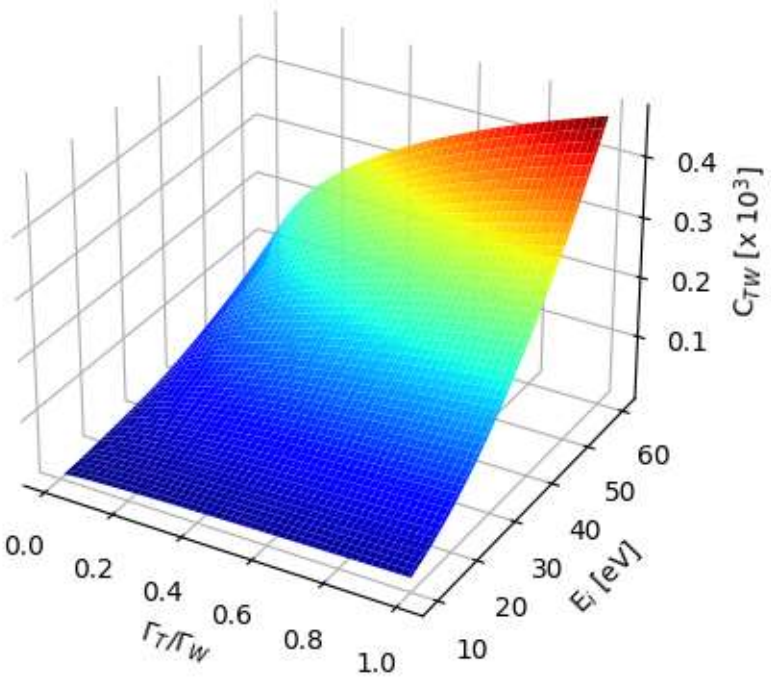

Figure 2 - Relative atomic concentration of tritium in tungsten co-deposited layers. Extrapolation of the correlation from [28]. T = 473 K.

A relative concentration of $C_{TW} \equiv C_{TW}(T = 473K) = 3.2 \cdot 10^{-5}$ is found from the calculations. C_{TW} shows an inverse dependence on T. For the highest allowable surface temperature of the divertor, $C_{TW}(T = 1373K) = 1.1 \cdot 10^{-5}$, about three times lower than $C_{TW}(T = 473K)$. Therefore, the concentration ranges between $3.2 \cdot 10^{-5}$ and $1.1 \cdot 10^{-5}$. The value $C_{TW} = 3.2 \cdot 10^{-5}$ is used as conservative assumption. The reader should be aware that this is probably an overestimate of the real concentration. For a more precise quantification of the uncertainties, a sensitivity analysis has been performed. The exponents α, β in the correlation (Eq. (2)) have been varied in their validity range (Eq. (5)). Figure 3 shows the results of the sensitivity analysis. A maximum value of the relative concentration $C_{TW,max} = 1.75 \cdot 10^{-4}$ is found for $\alpha = 0.30, \beta = 2.25$.

$$C_{TW}(\alpha, \beta) = 5.13 \cdot 10^{-8} \cdot \left(\frac{\Gamma_T}{\Gamma_W}\right)^{\alpha} \cdot E_n^{\beta} \cdot exp\left(\frac{736 \pm 228}{T}\right) \quad (5)$$

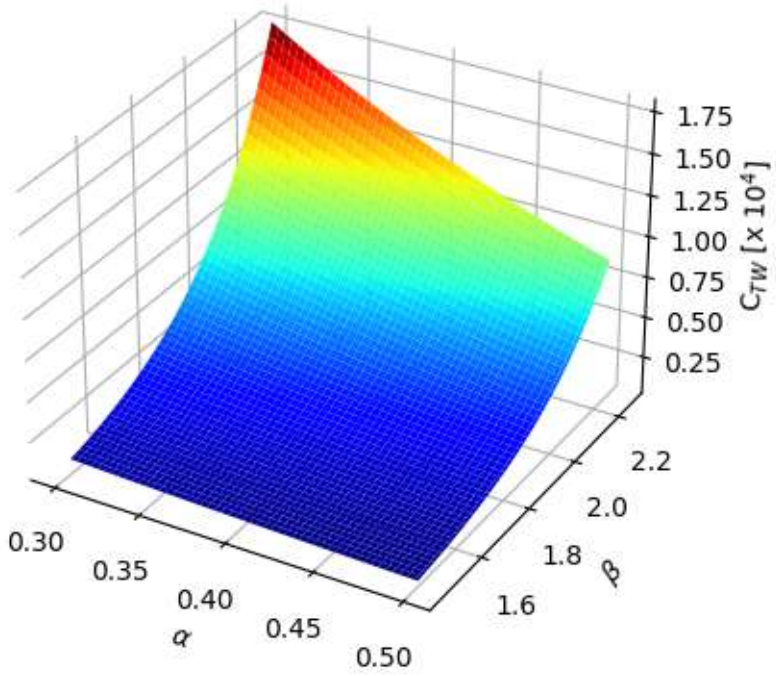

Figure 3 - Sensitivity analysis on the exponents in Eq. (2). Tritium concentration in tungsten spans for about one order of magnitude. T = 473 K.

Finally, the mass of tritium in co-deposited tungsten is quantified. The co-deposited tungsten mass is estimated as 90% of the tungsten mass that is eroded during operations, $M_{W,codep} = 81\ g/y$ (see Section 4.4). This value rises to $M_{W,codep} = 101.3\ g/y$ if self-sputtering is considered, as described in Section 3. After one year at full power (i.e., in the operational period from the 9th year to the 28th), the tritium mass is:

$$M_{T,codep} = C_{TW} M_{W,codep} = 3.3\ mg \quad (6)$$

where $M_{W,codep}$ is the mass of co-deposited tungsten, and $C_{TW} = 3.2 \cdot 10^{-5}$ is the value of tritium concentration for DTT operating conditions. An upper bound of the tritium mass can be computed from the maximum tritium concentration, $C_{TW,max} = 1.75 \cdot 10^{-4}$ (Figure 3). In that case, $M_{T,codep,max} = 17.9\ mg$. $M_{T,codep,max}$ is larger than the amount of tritium produced in the vacuum chamber in one year

($2.8\ TBq$, equivalent to $7.8\ mg$). This means that a) the correlation developed by [28] gives unphysical results outside its range of validity or b) such a concentration ($C_{TW,max}$) is reached in more than a year.

Since tungsten belongs to mobility category IV [29] (i.e., 10% would be mobilized in case of severe accidents), the mobilizable tritium inventory from co-deposited tungsten is $M_{T,codep,mob} = 0.33\ mg$.

4.3 Tritium implanted

The amount of tritium implanted is computed according to Eq. (4). Divertor and first wall have been considered separately, with the respective surfaces $S_{div} = 20\ m^2$, $S_{FW} = 66.8\ m^2$. Detailed calculations have been performed by taking advantage of the TRIM code [38], considering an incident angle of 88° with respect to the normal of the divertor plates. The sheaths effect on the angle of incidence of the ions are not considered. A mean implantation depth of $0.8\ \mu m$ is found from TRIM simulations. Nevertheless, a sensitivity analysis has been performed on C_{TW} and d_{imp}. C_{TW} is assumed in the range $[10^{-5}; 10^{-2}]$, while the implantation depth ranges from $0.8\ \mu m$ to $10\ \mu m$. Results are shown in Figure 4 and Figure 5.

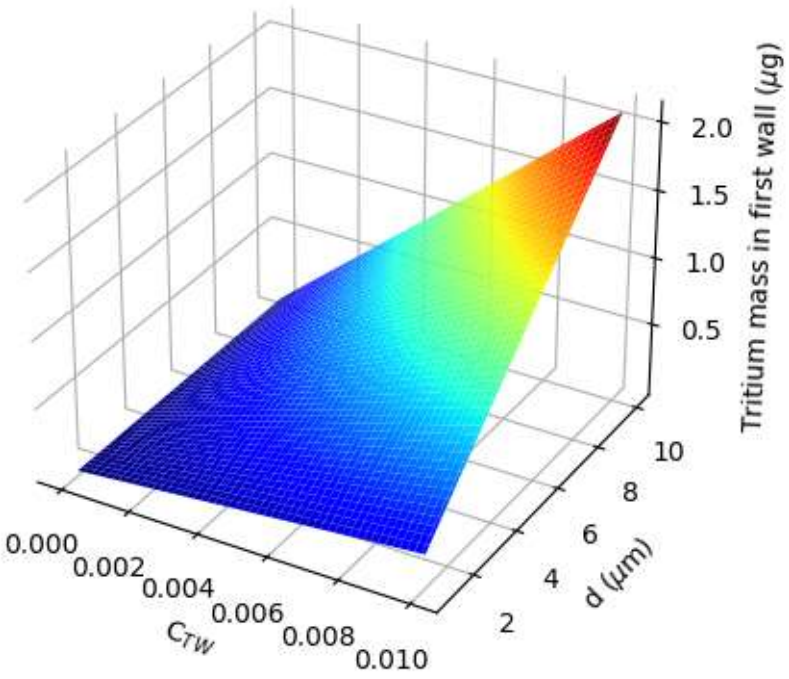

Figure 4 - Tritium mass in the first wall as a function of implantation depth and tritium concentration in tungsten. T = 473 K.

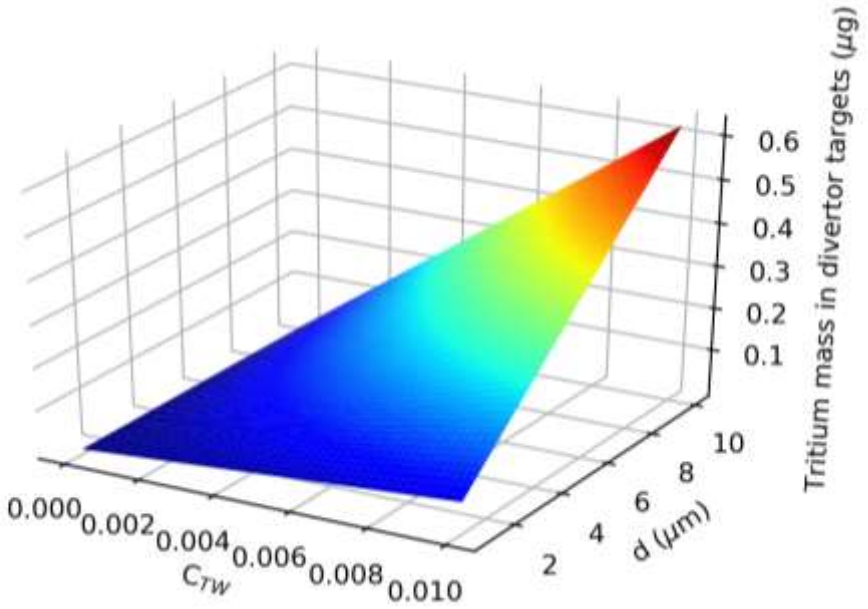

Figure 5 - Tritium mass in the divertor as a function of implantation depth and tritium concentration in tungsten. T = 473 K.

For $d_{imp} = 0.8\,\mu m$ and $C_{TW} = 10^{-2}$, the tritium implanted is $M_{T,FW} = 0.16 \cdot 10^{-3}\,mg$, $M_{T,div} = 0.048 \cdot 10^{-3}\,mg$. Tritium may also diffuse beyond the implantation depth. However, the concentration beyond the implanted zone is much lower, showing negligible values above $100\,\mu m$ [4]. In a worst-case scenario that considers a $C_{TW} = 10^{-2}$ up to $100\,\mu m$ in tungsten, $M_{T,FW} = 0.21\,mg$, $M_{T,div} = 0.063\,mg$. Additional consideration may be made on the value of C_{TW} in the FW and the divertor. As a matter of fact, a lower concentration in the FW is expected due to the lower ion flux if compared to the divertor targets. The values of $M_{T,FW} = 0.21\,mg$, $M_{T,div} = 0.063\,mg$ provide a huge conservative margin. Therefore, they will be used as reference for the source term, keeping in mind that a more realistic value is provided by $M_{T,FW} = 0.16 \cdot 10^{-3}\,mg$, $M_{T,div} = 0.048 \cdot 10^{-3}\,mg$. The mobilizable inventory of the implanted tritium depends on the accidental scenario conditions. Assuming again 10% of mobilizable fraction, $M_{T,imp,mob} = 27\,\mu g$. It should be noted that mobilizing the tritium in the tungsten bulk requires severe accidental conditions. A 10% mobilizable fraction is a conservative assumption.

4.4 Activated dust

Tungsten erosion has been computed on the 35 divertor nodes for deuterium, tritium and neon ions. Deuterium ions at $14.39\,eV$ produces a negligible sputtering, even considering the acceleration in the Debye sheath. Neon ions produces a negligible sputtering below a threshold energy $\sim 10\,eV$. The highest energy reached by Ne^{10+} is approximately 450 eV. At these energies, the sputtering yield of Ne on W target is considerable. Tritium ions at 1 MeV have been considered as well. As a matter of fact, energetic tritium ions will be generated by the D-D reactions. The sputtering yield for tritium ions at 1 MeV is comparable to medium energy Ne ions. However, the tritium ion flux is considerably lower. Even assuming that all the tritons collide with the target, the triton flux is at least three orders of magnitude lower than deuterium and ions flux. The eroded tungsten flux from D and Ne ions at $T = 14.39\,eV$ and T ions at $T = 1MeV$ is respectively $\Gamma_{ero,D} \approx 0$, $\Gamma_{ero,Ne} = 1.08 \cdot 10^{19}\,atoms/s$ and $\Gamma_{ero,T} = 6.27 \cdot 10^{15} atoms/s$. Tungsten erosion on the first wall results negligible because of the low energy of ions impacting on W. Transient events have been considered as well by comparison with JET operations. In JET-ILW it was found that the sputtered particles from high energy deuterium ions (1 keV) during ELMs is approximately five times the sputtered particles from impurities during nominal operations. Also, ELMs frequency of occurrence is 0.01 (10 ms for every second of operation) [19]. Hence, as an effect of W erosion due to sputtering by ELMs, $11\,g$ of tungsten dust could be

produced due to DTT operations. Clearly, DTT operating parameters will not match exactly the JET-ILW conditions reported in [19]. Also, the model exploited for JET-ILW is affected by uncertainty due to the impossibility to simulate exactly the transient intra-ELMs. Yet, this approach provides a rough estimate of the dust that might be produced in DTT during ELMs. As a results, the total dust mass at the end-of-life amounts to $290\ g$. We recall that the contribution from disruptions is not considered in this work. Also, in the present model the activated dust mass is directly proportional to the redeposition probability, as described in Section 3.4. The value $p = 0.9$ was chosen to provide a small conservative margin ($\sim 5\%$) with respect to experimental findings in conditions similar to the ones expected in DTT. Post-mortem analysis in JET reported $p > 0.94$ [20]. If higher values of p are chosen, such as $p = 0.99$ as observed in [19], the dust mass drastically decreases to $29.0\ g$. Conversely, one can assume that also the tungsten that is redeposited may be mobilized during a severe accident. In this extremely conservative case, the mobilizable activated dust mass reaches $2.90\ kg$. Hence, the reader should be aware that dust mass may vary in the range $29.0 \div 2903\ g$.

The activity associated to the activated dust is shown in Figure 6. Data on W specific activity has been taken from [23]. Three cases are shown: dust activity after 18 months of operations (case 1), 42 months (case 2) and end of life (case 3). Tungsten activity after 6 months for case 1 and case 2 is negligible.

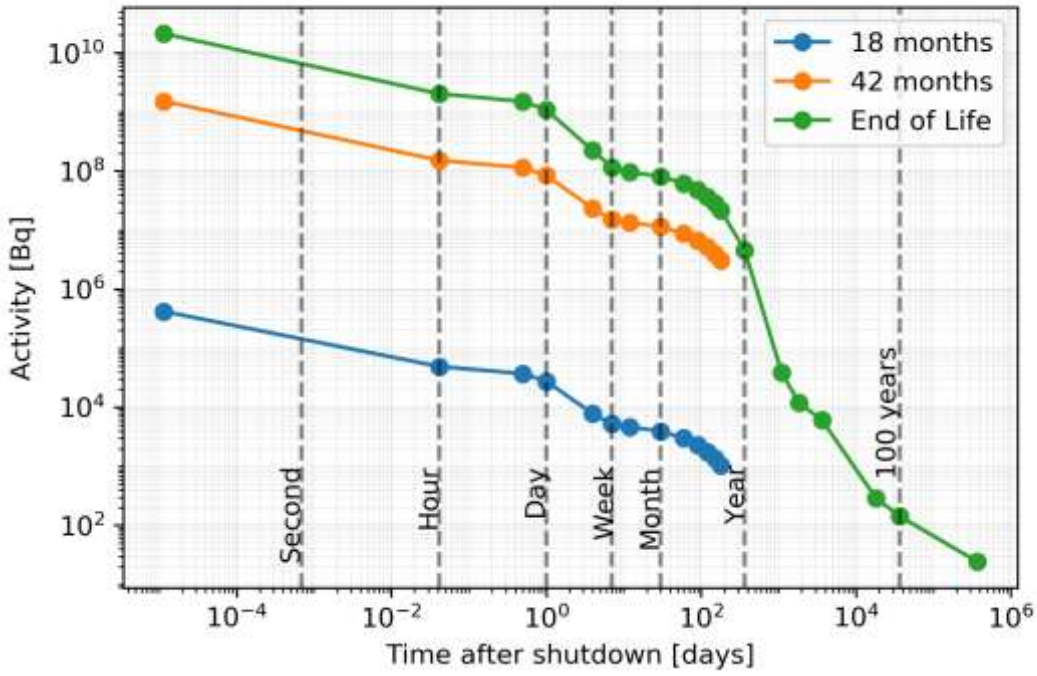

Figure 6 - Dust activity following reactor shutdown. Three cases have been considered: shutdown after 18 months, 42 months, end of life.

5. Discussion

Quantifying the radiological source terms for future fusion machines is a hard task. Nevertheless, it is a mandatory step for licensing the machines, and safety for workers, population and environment must be assessed. Strong simplifying assumptions have been made to compute the radiological source terms in DTT facility. From the safety viewpoint, these simplifying assumptions are balanced by a huge conservativism in the calculations. The results of the previous analysis are reported in Table 2.

A direct estimation of tritium concentration in re-deposited tungsten layer or implanted tritium is unpractical. Therefore, empirical correlations have been exploited. This allows to overcome modelling complexity for such phenomena, provided that the correlations are applicable for the problem under consideration. Actually, DTT operating parameters fall outside the range of validity of the correlations. Nevertheless, one can reasonably expect that a lower tritium energy or a lower tritium flux would lead to lower tritium concentrations in tungsten. Stated in a different way, no physical phenomena that can increase tritium concentration are expected at lower energies and fluxes with respect to the lower bound of the correlations. Furthermore, the whole amount of tritons produced is assumed to reach the walls. Such an assumption clearly overestimates the tritons flux impacting the walls. Therefore, the results can be considered conservative. The consistency of the approach for DTT has been also verified by comparison with other fusion machines. Similar ratio between tritium inventory and tritium input (injected as fuel for AUG and Alcator C-Mod, produced by D-D reactions for DTT) are found.

As far as dust production is concerned, more detailed input data were available for the analysis. Results from edge plasma simulations allowed to set up TRIM simulations for a precise estimation of the sputtering yield on divertor targets. The reader should be aware that results for the activated dust should be considered as work in progress. The sputtered tungsten atoms may be pumped out from the vacuum chamber before contributing to the dust production, reducing the total amount of dust. Conversely, disruptions in DTT may give a larger contribution to the dust production depending on their frequency and energy. Detailed calculation concerning disruptions in DTT are currently ongoing, and the dust production will be updated as the analyses proceed.

The results highlight the strong machine safety features. Tritium source terms are extremely low, for a total amount of tritium lower than one milligram after one year of full power operations. The activated dust amounts to 232 g at the end of life. Both those values meet the safety goals for the DTT facility.

Table 2 - Source terms mass and radioactivity.

Source term	**Mass [mg]**	**Radioactivity [Bq]**	**Notes**
Tritium in gaseous form in the vacuum chamber	$2.8 \cdot 10^{-2}$	10^{10}	Maximum value reached at the end of a shot
Tritium in co-deposited tungsten	3.3 (of which 0.33 mobilizable)	$1.2 \cdot 10^{12}$ (of which $1.2 \cdot 10^{11}$ mobilizable)	Yearly production. Equivalent to 1.2 TBq/y (of which 0.12 TBq/y mobilizable)
Tritium implanted in the FW	0.21 (of which 0.021 mobilizable)	$7.50 \cdot 10^{10}$ (of which $7.50 \cdot 10^{9}$ mobilizable)	Maximum value reached at steady state. (More likely value is $5.7 \cdot 10^{7}$ Bq, of which $5.7 \cdot 10^{6}$ Bq mobilizable.

			Computed with $d_{imp} = 0.8\ \mu m$)
Tritium implanted in the divertor	0.063 (of which 0.0063 mobilizable)	$2.25 \cdot 10^{10}$ (of which $2.25 \cdot 10^{9}$ mobilizable)	Maximum value reached at steady state. (More likely value is $1.7 \cdot 10^{7}\ Bq$, of which $1.7 \cdot 10^{6}\ Bq$ mobilizable. Computed with $d_{imp} = 0.8\ \mu m$))
Activated dust	$290 \cdot 10^{3}$ (mobilizable)	$2.11 \cdot 10^{10}$	Maximum value, reached at end of life.

6. Conclusions

DTT facility will start its operations in 2026. In the wide framework of safety analysis, a source terms quantification has been carried out in this work. The amount of tritium produced in a single shot is quite low. Even assuming that all this tritium is highly mobilizable (i.e., it is in gaseous form in the vacuum chamber), the expected consequences of an accidental release are minimal. Similarly, both the tritium implanted in the walls and the tritium in co-deposited tungsten layer is below 1 mg after one year of full power operations. A reasonable level of conservativism was chosen for the analysis, and the results provide an upper bound for more detailed analyses that will be carried out in the near future as the design of DTT proceeds Activated dust produced during inter ELM and intra ELM phases of steady state discharges amounts to 290 g at the end of life and the corresponding activity is comparable to that of tritium implanted. These values are probably to be increased when the effect of disruptions will be taken into account. The values presented in this work should be considered a preliminary estimation of DTT source terms. Detailed codes will be exploited to reduce the uncertainties on the source term estimations.

A deterministic analysis of possible accidental scenario is expected in the current year. An in-vessel LOCA (Loss Of Coolant Accident) will be simulated to assess the thermodynamic conditions reached in the VV due to the ingress of coolant. Therefore, the amount of radioactive material that can be mobilized will be assessed in a more precise way starting from the results presented in this work.

Acknowledgement

The authors thank all the members of the DTT HSEQ team for their precious advice and fruitful conversations.

References

[1] R. Martone, R. Albanese, F. Crisanti, A. Pizzuto, and P. Martin, “DTT Divertor Tokamak Test facility Interim Design Report, ENEA (ISBN 978-88-8286-378-4),” 2019, [Online]. Available: https://www.dtt-dms.enea.it/share/s/avvglhVQT2aSkSgV9vuEtw.

[2] A. Kirschner, V. Philipps, J. Winter, and U. Kögler, “Simulation of the plasma-wall interaction in a tokamak with the Monte Carlo code ERO-TEXTOR,” *Nucl. Fusion*, vol. 40, no. 5, p. 989, 2000.

[3] K. Schmid, K. Krieger, S. W. Lisgo, G. Meisl, S. Brezinsek, and J. E. T. Contributors, “WALLDYN simulations of global impurity migration in JET and extrapolations to ITER,” *Nucl. fusion*, vol. 55, no. 5, p. 53015, 2015.

[4] Y. Hatano *et al.*, “Trapping of hydrogen isotopes in radiation defects formed in tungsten by neutron and ion irradiations,” *J. Nucl. Mater.*, vol. 438, pp. S114–S119, 2013.

[5] C. H. Skinner *et al.*, “Recent Advances on Hydrogen Retention in ITER’s Plasma-Facing Materials: Beryllium, Carbon, and Tungsten,” *Fusion Sci. Technol.*, vol. 54, no. 4, pp. 891–945, Nov. 2008, doi: 10.13182/FST54-891.

[6] J. P. Coad *et al.*, “Overview of material re-deposition and fuel retention studies at JET with the Gas Box divertor,” *Nucl. Fusion*, vol. 46, no. 2, p. 350, 2006.

[7] A. Widdowson *et al.*, “Overview of the JET ITER-like wall divertor,” *Nucl. Mater. Energy*, vol. 12, pp. 499–505, 2017.

[8] K. Sugiyama *et al.*, “Tritium profile in plasma-facing components following D-D operation,” in *Journal of Nuclear Materials*, Aug. 2004, vol. 329–333, no. 1-3 PART A, pp. 874–879, doi: 10.1016/j.jnucmat.2004.04.345.

[9] W. J. Carmack, R. A. Anderl, R. J. Pawelko, G. R. Smolik, and K. A. McCarthy, “Characterization and

analysis of dusts produced in three experimental tokamaks: TFTR, DIII-D, and Alcator C-Mod," *Fusion Eng. Des.*, vol. 51, pp. 477–484, 2000.

[10] S. H. . "Hong *et al.*, "Temporal and Spatial Evolution of In-vessel Dust Characteristics in KSTAR and Dust Removal Experiments in TReD," 2012, doi: https://doi.org/.

[11] N. Ashikawa, N. Asakura, M. Fukumoto, T. Hayashi, Y. Ueda, and T. Muroga, "Characteristics of tungsten and carbon dusts in JT-60U and evaluation of hydrogen isotope retention," *J. Nucl. Mater.*, vol. 438, pp. S664–S667, 2013, doi: https://doi.org/10.1016/j.jnucmat.2013.01.140.

[12] S. V Gorman, W. J. Carmack, and P. B. Hembree, "Particle size distribution of dust collected from Alcator C-MOD," *Fusion Technol.*, vol. 34, no. 3P2, pp. 745–749, 1998.

[13] S.-H. Hong, C. Grisolia, V. Rohde, P. Monier-Garbet, T. S. Team, and A. U. Team, "Temporal evolution and spatial distribution of dust creation events in Tore Supra and in ASDEX Upgrade studied by CCD image analysis," *Nucl. fusion*, vol. 50, no. 3, p. 35002, 2010.

[14] M. Tang, J. S. Hu, J. G. Li, Y.-F. Li, G. Morfill, and N. Ashikawa, "Recent researches on dust in EAST and HT-7 tokamaks," *J. Nucl. Mater.*, vol. 415, no. 1, pp. S1094–S1097, 2011.

[15] V. Rohde, A. Kallenbach, V. Mertens, and R. Neu, "Wall retention of deuterium and gaseous impurities in all tungsten ASDEX Upgrade," *Plasma Phys. Control. Fusion*, vol. 51, no. 12, p. 124033, 2009, doi: 10.1088/0741-3335/51/12/124033.

[16] M. Balden *et al.*, "Collection strategy, inner morphology, and size distribution of dust particles in ASDEX Upgrade," *Nucl. Fusion*, vol. 54, no. 7, p. 73010, 2014.

[17] J. P. Sharpe *et al.*, "Characterization of dust collected from ASDEX-Upgrade and LHD," *J. Nucl. Mater.*, vol. 313, pp. 455–459, 2003.

[18] K. Masaki *et al.*, "Tritium distribution in JT-60U W-shaped divertor," in *Journal of Nuclear Materials*, Mar. 2003, vol. 313–316, no. SUPPL., pp. 514–518, doi: 10.1016/S0022-3115(02)01388-0.

[19] A. Kirschner *et al.*, "Modelling of tungsten erosion and deposition in the divertor of JET-ILW in comparison to experimental findings," *Nucl. Mater. Energy*, vol. 18, pp. 239–244, Jan. 2019, doi: 10.1016/j.nme.2019.01.004.

[20] S. Brezinsek *et al.*, "Erosion, screening, and migration of tungsten in the JET divertor," *Nucl. fusion*, vol. 59, no. 9, p. 96035, 2019.

[21] J. Guterl, I. Bykov, R. Ding, and P. Snyder, "On the prediction and monitoring of tungsten prompt redeposition in tokamak divertors," *Nucl. Mater. Energy*, vol. 27, p. 100948, Jun. 2021, doi: 10.1016/j.nme.2021.100948.

[22] D. Naujoks, *Plasma-material interaction in controlled fusion*, vol. 39. Springer Science & Business Media, 2006.

[23] R. Villari *et al.*, "Nuclear design of divertor tokamak test (DTT) facility," *Fusion Eng. Des.*, vol. 155, p. 111551, 2020.

[24] A. S. Richardson, "2019 NRL Plasma Formulary," US Naval Research Laboratory, 2019.

[25] K. K. Kirov *et al.*, "Synergistic ICRH and NBI heating for fast ion generation and maximising fusion rate in mixed plasmas at JET," in *AIP Conference Proceedings*, 2020, vol. 2254, no. 1, p. 30011.

[26] C. H. Skinner *et al.*, "Studies of tritiated co-deposited layers in TFTR," *J. Nucl. Mater.*, vol. 290, pp. 486–490, 2001.

[27] G. De Temmerman, M. J. Baldwin, R. P. Doerner, D. Nishijima, and K. Schmid, "An empirical scaling for deuterium retention in co-deposited beryllium layers," *Nucl. Fusion*, vol. 48, no. 7, p. 75008,

2008.

[28] G. De Temmerman and R. P. Doerner, “Deuterium retention and release in tungsten co-deposited layers,” *J. Nucl. Mater.*, vol. 389, no. 3, pp. 479–483, 2009, doi: 10.1016/j.jnucmat.2009.03.028.

[29] J. Holdren and L. L. Labs, “‘Summary of the Report of the Senior Committee on Environmental, Safety and Economic Aspects of Magnetic Fusion Energy,’” 1988.

[30] K. Huang, X. Zhao, B. Lyu, and S. Liu, “Evaluation of implantation-driven tritium transport in the first wall of the WCCB blanket for CFETR,” *Fusion Eng. Des.*, vol. 152, p. 111430, 2020.

[31] R. A. Causey and T. J. Venhaus, “The use of tungsten in fusion reactors: a review of the hydrogen retention and migration properties,” *Phys. Scr.*, vol. 2001, no. T94, p. 9, 2001.

[32] J. P. Sharpe, D. A. Petti, and H. W. Bartels, “A review of dust in fusion devices: Implications for safety and operational performance,” *Fusion Eng. Des.*, vol. 63–64, pp. 153–163, 2002, doi: 10.1016/S0920-3796(02)00191-6.

[33] W. J. Carmack, M. E. Engelhart, P. B. Hembree, K. A. Mc Carty, and D. A. Petti, “DIII-D dust particulate characterization,” *INEEL Extern. Rep. INEEL/EXT-97-00702*, 1997.

[34] A. T. Peacock *et al.*, “Dust and flakes in the JET MkIIa divertor, analysis and results,” *J. Nucl. Mater.*, vol. 266, pp. 423–428, 1999.

[35] C. Grisolia, S. Rosanvallon, A. Loarte, P. Sharpe, and C. Arnas, “From eroded material to dust: An experimental evaluation of the mobilised dust production in Tore Supra,” *J. Nucl. Mater.*, vol. 390–391, no. 1, pp. 53–56, 2009, doi: 10.1016/j.jnucmat.2009.01.045.

[36] P. Chappuis *et al.*, “Dust characterization and analysis in Tore-Supra,” *J. Nucl. Mater.*, vol. 290, pp. 245–249, 2001.

[37] J. P. Sharpe, P. Chappuis, and D. A. Petti, “Characterization of tokamak dust collected from Tore Supra,” *Fusion Technol.*, vol. 39, no. 2P2, pp. 1061–1065, 2001.

[38] J. F. Ziegler, M. D. Ziegler, and J. P. Biersack, “SRIM–The stopping and range of ions in matter (2010),” *Nucl. Instruments Methods Phys. Res. Sect. B Beam Interact. with Mater. Atoms*, vol. 268, no. 11–12, pp. 1818–1823, 2010.

[39] M. Z. Tokar, “An assessment for the erosion rate of DEMO first wall,” *Nucl. Fusion*, vol. 58, no. 1, p. 16016, 2017.

[40] C. Ostrouchov, Y. Zhang, and J. Weber, “Pysrim: automation, analysis, and plotting of SRIM calculations,” *J. Open Source Softw.*, vol. 3, no. 28, 2018.